# Modelling the fretting fatigue crack growth: From short crack correction strategies to microstructural approaches

Alix De Pannemaecker, Siegfried Fouvry, Jean-Yves Buffiere, Myriam Brochu

# Modelling the fretting fatigue crack growth: from short crack correction strategies to microstructural approaches

A. de Pannemaecker[a,*], S. Fouvry[a,*], J.Y. Buffiere[b], M. Brochu[c]

[a] LTDS, Ecole Centrale de Lyon, 69130 Ecully, France
[b] MATEIS, INSA de Lyon, 69621 Villeurbanne, France
[c] Département génie Mécanique, Ecole Polytechnique de Montréal, QC H3T 1J4, Montréal, Canada

Corresponding authors:
adepannemaecker@gmail.com
siegfried.fouvry@ec-lyon.fr

**Abstract**

Predicting the fretting fatigue crack propagation is complex and uncertain. It implies to consider stress gradient and short crack behavior. To address this challenge former in situ synchrotron X-ray imaging of micro-fretting fatigue experiments are simulated. First a Pugno *et al.* / Fleury *et al.* short crack correction (SCC) approach is considered. Then a microstructural Navarro-Rios (NR) model originally developed to analyze fatigue crack growth for short crack is transposed. Both strategies are compared. Very good agreement with experiments are observed. However the NR model provides a more physical description of the short crack behavior allowing the quantification of the non-monotonous crack growth rate when this later shifts from fretting dominant to fatigue dominant stress domain.

**Keywords:** Fretting fatigue; Crack growth propagation; In situ tests; Short cracks; Fatigue life

## 1. Introduction

First studied by Eden [1], fretting is defined as a small oscillatory movement between two surfaces in contact. When combined with fatigue loadings, the crack nucleated by fretting stresses can propagate until failure of the structure [2-4]. When cracking mechanisms are involved in fretting configurations, the fretting life can be split into three different phases: a crack nucleation period which corresponds to the formation of microcracks mainly controlled by the cyclic fretting contact stresses [5], a crack growth period corresponding to the transition from micro- to macrocracks. First controlled by the contact stress the crack extension is progressively driven by the bulk fatigue loading. Note that a crack arrest condition can be achieved in the short or the long crack regime depending on the combined fretting and fatigue stressing conditions [6]. From this analysis, it was shown that fretting, by favoring the crack nucleation and promoting an initial crack propagation can drastically reduce the fatigue endurance of assemblies [7]. When the crack growth rate is within the Paris region, for fretting fatigue tests, a competition between fretting and fatigue will occur leading to higher crack growth rates than with simple fatigue tests. On the contrary, if the crack tip is far enough from

the contact, fretting loads have no influence any more on the crack tip, meaning that crack growth rates will be identical for fretting fatigue and fatigue tests within the Paris region.

Fretting fatigue crack prediction requires non-local multiaxial fatigue criteria to capture the stress gradient and complex state imposed by the contact loading [8-11]. In order to model the crack growth propagation, LEFM approach under mixed mode loading conditions is usually considered. A modified Paris relation is adopted defining an equivalent stress intensity factor $K_{eq}$ taking into account the mode I and mode II components. Combining crack nucleation and propagation, the global fretting fatigue life can be evaluated [12-14]. Rather good correlations are usually observed. One limitation of this model concerns the crack path prediction. The crack growth prediction deals with two issues: the crack path determination and the crack growth rate. Recently Baietto *et al.* propose a global-local strategy based on the XFEM (extended finite element method) which takes into account scale effects, structure, components, the contact interface, created cracks and interfacial non-linearities occurring within the crack lips [15]. A mixed mode Paris crack growth relation is introduced for plain fretting and preloaded fretting cracking configurations. Then the Hourlier [16] criterion is applied to determine the propagation direction of the crack and a very good correlation is observed. Another limitation of the LEFM approach concerns the short crack propagation description. Recently a short crack propagation strategy extracted from the El Haddad *et al.* approach was introduced by Fleury *et al.* to capture the stress gradient effect in notched specimen [17]. This approach will be examined in the present fretting fatigue analysis. However such approach is questionable from a physical point of view.

To overcome those limitations, the present work proposes another approach based on the Navarro-Rios formulations [18-20] and some extensions proposed by Vallellano *et al* [21-24]. A micromechanical model based on the Crack Tip Opening Displacement (CTOD) calculations, originally formulated for fatigue configurations, is extended to implement fretting effects. The model is considering both short and long crack regimes, takes into account high stress gradient effects, a variable stress ratio $R$ and the geometry of the specimen. The model is compared to 7050-T7451 aluminum alloy experimental data obtained using in situ small-scale fretting fatigue setup especially developed to fit within the synchrotron facility (ESRF, Grenoble, France).

**Nomenclature**

| | |
|---|---|
| $a$ | Crack length (m) |
| $a_0$ | Short crack/long crack transition (m) |
| $A_1$ | Coefficient describing the Paris region ($m/(cycle.MPa\sqrt{m})$) |
| $A_2$ | Coefficient describing the Navarro-Rios model ($1/cycle$) |
| $b$ | Half width of the contact area (m) |
| $D$ | Average grain size (m) |
| $da/dN$ | Crack growth rate (m/cycle) |
| | Young's modulus (Pa) |
| $'$ | Young's modulus corresponding to plane strain conditions (Pa) |
| $(\%)$ | Relative error (%) |
| $f$ | Material dependent parameter (-) |
| $f(z/a)$ | Polynomial function determined by the FEM (-) |

| | |
|---|---|
| $F$ | Fatigue load (N) |
| $F_a$ | Fatigue amplitude (N) |
| $F_a^*$ | Maximum fatigue amplitude (N) |
| $F_m$ | Average fatigue load (N) |
| $i$ | Parameter corresponding to a certain state (-) |
| $K$ | Stress intensity factor ($MPa\sqrt{m}$) |
| $K_{eq}$ | Equivalent stress intensity factor ($MPa\sqrt{m}$) |
| $K_{th}$ | Long crack stress intensity factor threshold ($MPa\sqrt{m}$) |
| $m_1$ | Exponent describing the Paris region (-) |
| $m_2$ | Exponent describing the Navarro-Rios model (-) |
| $m_{SC}$ | Exponent describing the Short Crack Correction model (-) |
| $N$ | Number of cycles (-) |
| $N_f$ | Number of cycles at failure (-) |
| $NR$ | Related to the Navarro-Rios model |
| $n_1$ | Non-dimensional crack length (-) |
| $n_2$ | Non-dimensional crack length located at a grain boundary (-) |
| $n_1^i\big\vert_C$ | Critical non-dimensional crack length (-) |
| $n_2^i\big\vert_C$ | Critical non-dimensional crack length located at a grain boundary (-) |
| $P$ | Linear normal load (N/m) |
| $p$ | Surface pressure (Pa) |
| $p_{max}$ | Maximum surface pressure (Pa) |
| $Q$ | Fretting linear tangential load (N/m) |
| $Q^*$ | Fretting linear tangential load amplitude (N/m) |
| $q$ | Surface shear (Pa) |
| $q_{max}$ | Maximum surface shear (Pa) |
| $R$ | Stress ratio (-) |
| $R_a$ | Surface roughness (m) |
| $R_{eq}$ | Equivalent stress ratio (-) |
| $R_{fa}$ | Stress ratio related to the fatigue load (-) |
| $R_{fr}$ | Stress ratio related to the fretting load (-) |
| $r$ | Radius of the fretting pad (m) |
| $r_0$ | Distance of the first dislocation located after a grain boundary (m) |
| $SCC$ | Related to the Short Crack Correction model |
| $Y_i$ | Correction factor (-) |
| $z$ | Depth (m) |
| *Greek letters:* | |
| $\Delta K$ | Stress intensity factor range ($MPa\sqrt{m}$) |
| $\Delta K_{eq}$ | Equivalent stress intensity factor range ($MPa\sqrt{m}$) |
| $\Delta K_{th}$ | Long crack stress intensity factor range threshold ($MPa\sqrt{m}$) |
| $\Phi$ | Crack tip opening displacement (m) |
| $\mu_{crack}$ | Friction coefficient within the crack lips (-) |

| | |
|---|---|
| $\mu_t$ | Friction coefficient at the sliding transition (-) |
| $\upsilon$ | Poisson coefficient (-) |
| $\sigma$ | Stress (Pa) |
| $\sigma_a$ | Fatigue stress amplitude (Pa) |
| $\sigma_{eq}$ | Equivalent stress (Pa) |
| $\sigma_{th}$ | Maximum stress threshold (Pa) |
| $\sigma_u$ | Ultimate stress (Pa) |
| $\sigma_y$ | Yield stress (Pa) |
| $\sigma_{0.2}$ | Conventional yield stress at 0.2% (Pa) |
| $\sigma_1$ | Stress opposed to the crack tip opening and closing (Pa) |
| $\sigma_2$ | Stress opposed to deformation (Pa) |
| $\sigma_3$ | Stress needed for a crack to propagate (Pa) |
| *Subscripts:* | |
| $CI$ | Related to the Contour Integral Method (Rice's integrals) |
| $eq$ | Related to an equivalent state |
| $max$ | Related to a maximum state |
| $min$ | Related to a minimum state |
| $SC$ | Related to a Short Crack description |
| $th$ | Related to a threshold state |
| $I$ | Related to a mode I propagation |
| $II$ | Related to a mode II propagation |
| $+Q^*$ | Related to a state at the maximum fretting tangential load |
| $-Q^*$ | Related to a state at the minimum fretting tangential load |

## 2. Small-scale fretting fatigue experiments

### *2.1. Material*

The present analysis was performed on the 7050-T7451 aluminum alloy widely used in aeronautical structures. Its chemical composition and mechanical properties are exposed in

Table 1 and Table 2. This alloy displays a mixed structure of non-recrystallized and recrystallized grains fully detailed in [25]. Large grains display an average grain size about $50-80\mu m$ whereas small ones are about $10-20\mu m$. Note that the average grain size along the transverse direction (T) for our configuration is about $D=30\mu m$ and will be used in the model later on.

Fretting fatigue specimens were extracted from a rolled aluminum block with 530mm along the longitudinal direction (L), 910mm along the transverse direction (T) and 110mm along the short direction (S). All samples were machined using electrical discharge machining and were manually polished to reach a low surface roughness ($R_a < 0.5\mu m$). Machining was chosen in order to apply the fretting fatigue load along the L-direction making the crack propagate along the T-direction. The cylindrical fretting pad, displaying a low surface roughness of $R_a = 0.5\mu m$,

is a heat treated 52100 steel ensuring that the crack only initiates and propagates within the aluminum samples.

Table 1: Chemical composition (wt.%) of the 7050-T7451 aluminum alloy [25]

| Si | Fe | Cu | Mn | Mg | Ti | Zn | Zr | Al |
|---|---|---|---|---|---|---|---|---|
| 0.28 | 0.19 | 1.76 | 0.07 | 2.42 | 0.06 | 6.15 | 0.14 | Bal |

Table 2: Mechanical properties of the two studied materials

| Material | $(GPa)$ | $\nu$ | $\sigma_{0.2}(MPa)$ | $\sigma_u(MPa)$ |
|---|---|---|---|---|
| 7050-T7151 [26] | 73.4 | 0.33 | 460 | 525 |
| 52100 [27] | 200 | 0.3 | 813 | 1500 |

The fretting fatigue experiment was done using a fatigue stress ratio around $R_{fa} \approx 0.3$. Unfortunately we do not display the fatigue limit at the same stress ratio for our aluminum alloy. This value is however known for the same orientation L-T at $R_{fa} = 0.0$ with $\sigma_{fl} \approx 120MPa$ and at $R_{fa} = 0.5$ with $\sigma_{fl} \approx 60MPa$ [28]. Therefore we will assume an intermediate value, so to say $\sigma_{fl} = 80MPa$. We previously performed fatigue crack growth tests on C(T) specimens at $R_{fa} = 0.3$ [29] leading to a long crack stress intensity factor range threshold of $\Delta K_{th} = 1.8MPa\sqrt{m}$ and a maximum stress intensity factor threshold of $K_{th} = 2.57MPa\sqrt{m}$. Applying the Kitagawa Takahashi approximation, the $a_0$ short crack transition is evaluated around:

$$a_0 = \frac{1}{\pi}\left(\frac{K_{th}}{\sigma_{fl}}\right)^2 = 162\mu m \qquad (1)$$

Hence the material properties related to studied fretting fatigue experiments are compiled in Table 3.

Table 3: Studied fretting fatigue experiments

| Material | $(GPa)$ | $\nu$ | $\sigma_{0.2}$ $(MPa)$ | $\sigma_{fl}$ $(MPa)$ $(R_{fa} = 0.3)$ | $a_0$ $(\mu m)$ $(R_{fa} = 0.3)$ | $\Delta K_{th}$ $(MPa\sqrt{m})$ $(R_{fa} = 0.3)$ | $K_{th}$ $(MPa\sqrt{m})$ $(R_{fa} = 0.3)$ |
|---|---|---|---|---|---|---|---|
| 7050-T7151 [28, 29] | 73.4 | 0.33 | 460 | 80 | 162 | 1.8 | 2.57 |
| 52100 [27] | 200 | 0.3 | 813 | N/A | N/A | N/A | N/A |

### *2.2. Experimental setup*

If both crack nucleation and crack arrest conditions are now well formalized through close correlations between experiments and simulations, the prediction of the crack propagation rate under complex fretting fatigue stressing remains a very challenging problem. In contrast to

crack nucleation and crack arrests which can be investigated using post mortem destructive observations measurement of the crack propagation rate requires in situ characterization of the crack extension. This is a complex experimental issue as in fretting fatigue the presence of the contact prevents a direct observation of the specimen surface. Fretting fatigue crack propagation rates can be measured using post mortem examination of several specimens obtained for several contact loading conditions and test durations [15]. In addition of being very tedious this experimental approach induces a relatively large scatter on the measured crack lengths which critically influences the crack rate calculation and cannot allow optimal modelling analysis. The potential drop method extensively applied in standard fatigue propagation experiments can also be used for fretting and fretting fatigue experiments [30] with the help of a calibration curve, crack propagation rates can be measured. However, in contrast to fatigue configurations, the presence of the contact pad induces a large scatter of the potential drop measurements so that only semi-quantitative estimation of the crack propagation rate can be extracted [30].

To overcome those limitations, one promising technique consists in performing X-ray tomography or radiography during a fretting fatigue test. An original device was specially developed by the MATEIS and LTDS laboratories in order to perform in situ fretting fatigue tests for the first time using synchrotron radiographic images [31].

Figure 1 shows the fretting fatigue setup principle (Figure 1.a) and its implementation within the synchrotron facility (ESRF, ID19 beamline, see Figure 1.c and Figure 1.d). The aluminum sample (Figure 1.b) is clamped at its top and bottom where the upper grip is fixed and the lower one mobile, in order to apply the cyclic fatigue loading at positive stress ratios $R_{fa} > 0$. A hydraulic actuator is used to generate the fatigue $F_m \pm F_a$ with $F_m = (F_{min} + F_{max})/2$ the average load, and $F_a = F_{max} - F_m$ the amplitude. To apply alternated fretting tangential force, a static normal force $P$ is imposed by the fretting pad on the specimen side. Bimetallic flexure elements are controlling the stiffness pad holder. Therefore the tangential load $\pm Q$ is created by both the sample elongation due to fatigue and the controlled stiffness of the fretting pad holder. The axial fatigue loads are recorded using $sensor_1 output$ and $sensor_2 output$ shown on Figure 1.a while the tangential load $Q$ is calculated with $Q = sensor_1 output - sensor_2 output$.

The crack nucleation and propagation were studied using 2D radiographs. Although this type of imaging provides an integrated view of damage though the specimen thickness, the geometry of the mechanical tests makes very difficult 3D tomographic imaging for which the sample should be exposed to the X-ray beam during a rotation of 180° (parallel beam). In order to fit within the synchrotron facility and because of the small maximum voxel available (pixel size of $0.72\mu m$ for a 2D view of an area about $1.5mm * 1.8mm$), the fretting fatigue device had to be considerably reduced compared to usual macroscopic tests. Therefore in order keep the plane strain hypothesis, the sample cross section was chosen to be of $2mm * 2mm$ with the following loading parameters: the linear normal force $P = 45N/mm$ generating a maximum hertzian pressure of $p_{max} = 300MPa$, and the cylinder pad radius is $r = 10mm$ leading to a $b = 0.099mm$ hertzian half contact width (distance from contact border to center). Finally the friction coefficient at the fretted interface $\mu_t = 1.3$ was obtained thanks to variable displacement tests [31].

For the following analysis, we are focusing on the partial slip condition corresponding to the regime generating cracks in fretting. This condition is fulfilled as long as the maximum tangential load amplitude $Q^*$ is relatively small compared to the normal load $P$ so that $Q^*/P \ll \mu_t = 1.3$.

Figure 2 summarizes the procedure to extract 2D-radiographic images taken at the synchrotron facility. The beam was pointed on the aluminum sample along the S-direction with its window covering the contact area, enabling images acquisition of the fretting fatigue crack propagation. A full analysis of the first results was previously completed, so that you can refer to [31] for additional information on the setup and test procedure. Note that radios obtained from Test A were previously analyzed in [31] as well so that only major results will be reminded in this paper for the sake of the discussion.

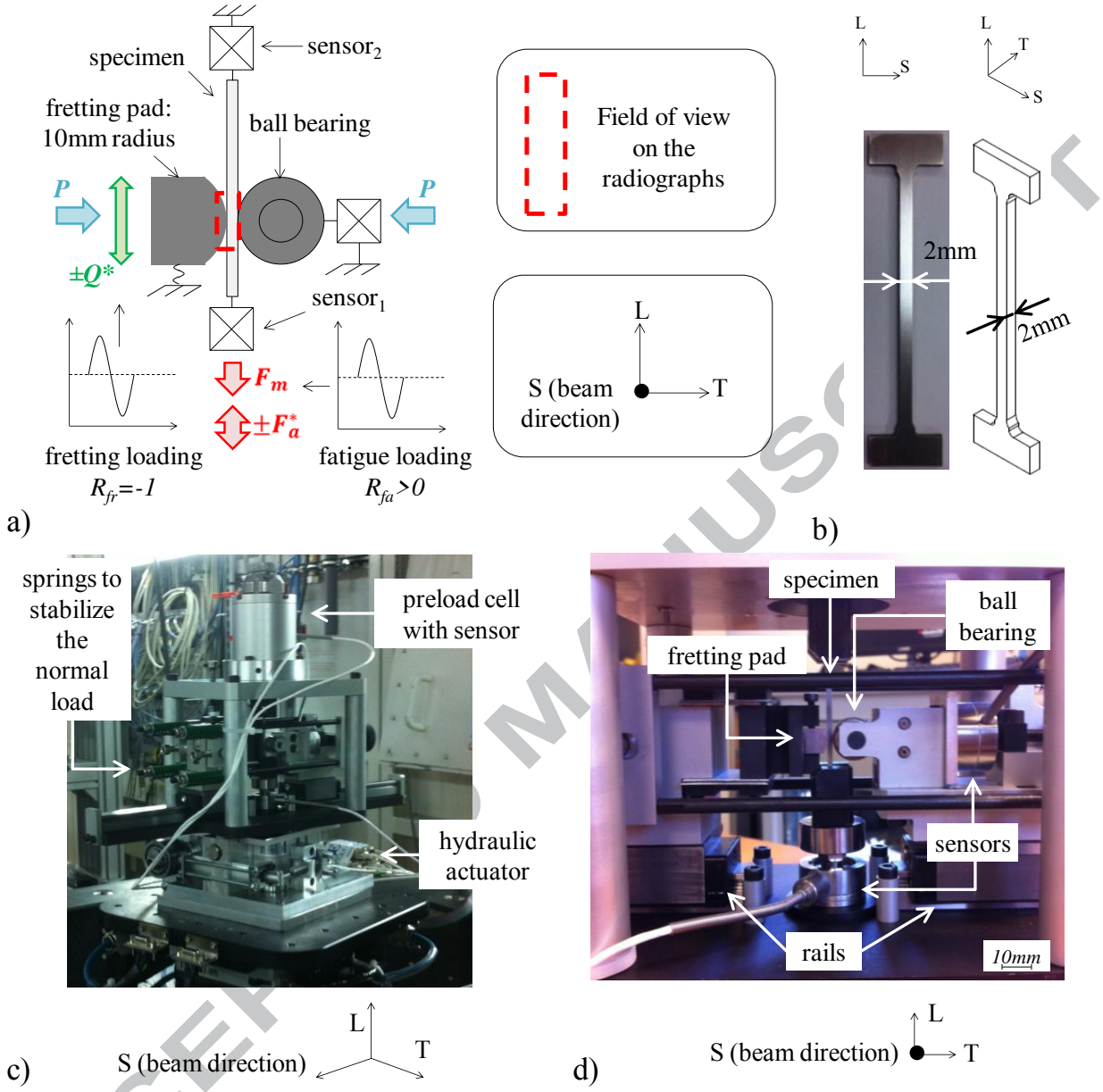


Figure 1: Micro fretting fatigue device (a) schematic diagram of the setup, (b) specimen geometry, (c) global view at the ESRF on ID19 beamline, (d) zoom on the contact [31]

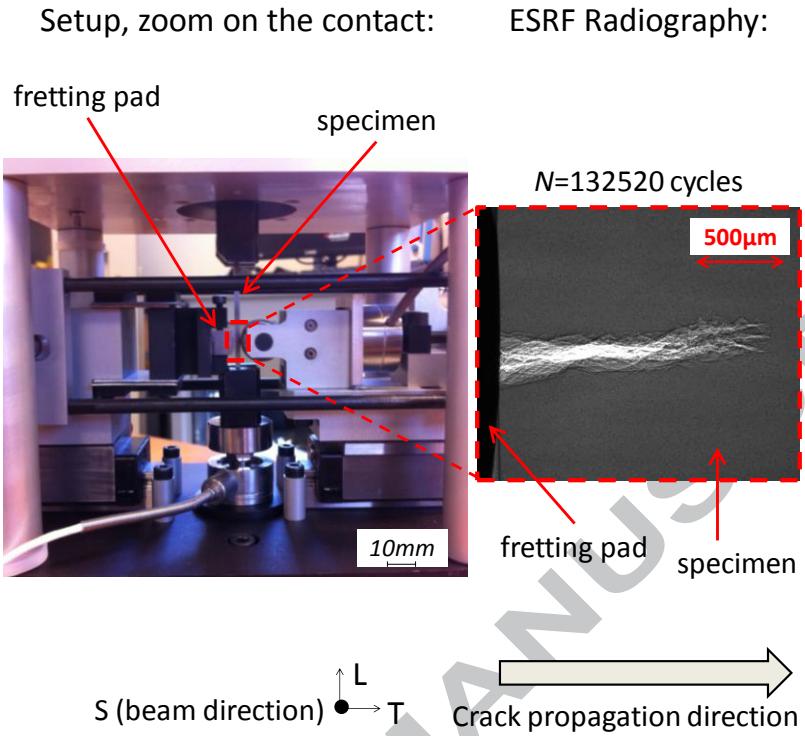


Figure 2: Zoom on the contact with a 2D-radiographic image taken at the ESRF (Test A: normal load $\boldsymbol{P = 45N/mm}$, maximum tangential load $\boldsymbol{Q = 38.5N/mm}$, fatigue amplitude $\boldsymbol{\sigma_a = 59.6MPa}$, fatigue stress ratio $\boldsymbol{R_{fa} = 0.29}$, number of cycles at failure $\boldsymbol{N_f = 132521}$ ) [31]

### *2.3. Experimental results*

Many tests were performed to adjust the procedure and optimize the cylinder/plane alignment which is a key aspect to generate reliable fretting fatigue cracking data. The present investigation focuses on two tests conditions A and B for which a perfect contact alignment was obtained (Table 4). Test A was performed with radio observations allowing the crack propagation rate analysis. This online analysis is compared to post mortem SEM and 3D surface profiles observations of the cracked surface. Test B was performed without radio observations so only post mortem expertises were achieved.

Both X-ray radio and post mortem crack extension analyses of test condition A are illustrated in Figure 3 and Figure 4 where the projected crack length $a$ along the vertical axis is plotted versus the fretting cycles.

By analyzing the radios taken from the micro fretting fatigue tests, the crack nucleation is quite hard to evaluate. After about 20000 fretting fatigue cycles, it is assumed that a through crack is obtained as the crack becomes clearly visible on the radios. The length of the first through crack is extended to be of the order of 100µm.

Table 4: Micro fretting fatigue test configurations ($\boldsymbol{r = 10mm, P = 45N/mm, p_{max} = 300MPa, \mu_t = 1.3}$)

| Test | $Q^*$ $(N/mm)$ | $q_{max}$ $(MPa)$ | $\sigma_{min}$ $(MPa)$ | $\sigma_{max}$ $(MPa)$ | $\sigma_a$ $(MPa)$ | $R_{fa}$ | $N$ at failure |
|---|---|---|---|---|---|---|---|
| A | 38.5 | 310 | 48.3 | 167.5 | 59.6 | 0.29 | 132521 |
| B | 36.0 | 302 | 53.3 | 162.0 | 54.4 | 0.33 | 179301 |

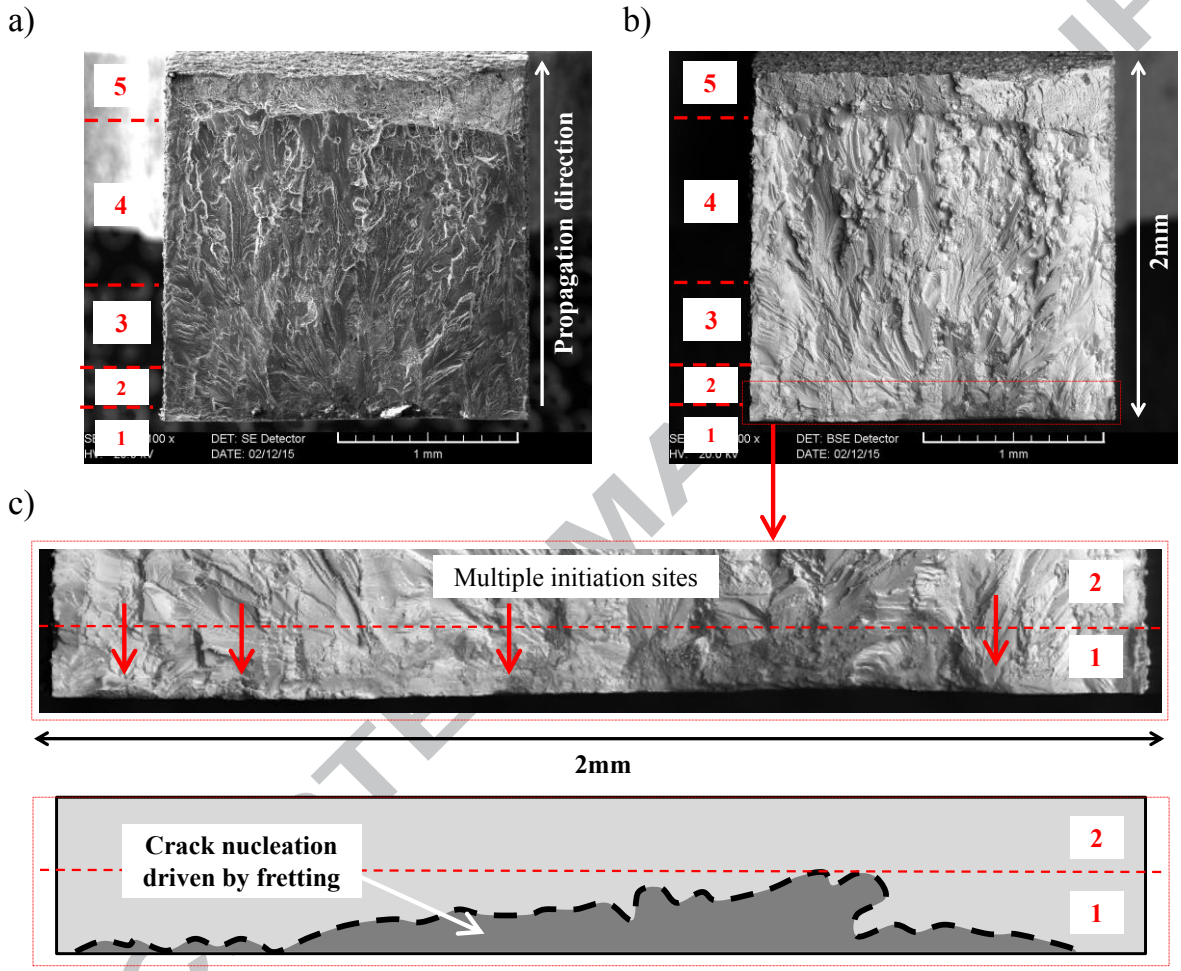


Figure 3: SEM observations of the fracture surfaces of the sample broken during Test A (a) secondary electron mode (b) back scattered electron mode (c) zoom (arrows indicate different crack initiation sites) and schematic description of the nucleation zone due to fretting ($\boldsymbol{p_{max} = 300MPa, q_{mqx} = 310MPa, \sigma_a = 59.6MPa, R_{fa} = 0.29, N_f = 132521}$) [31]

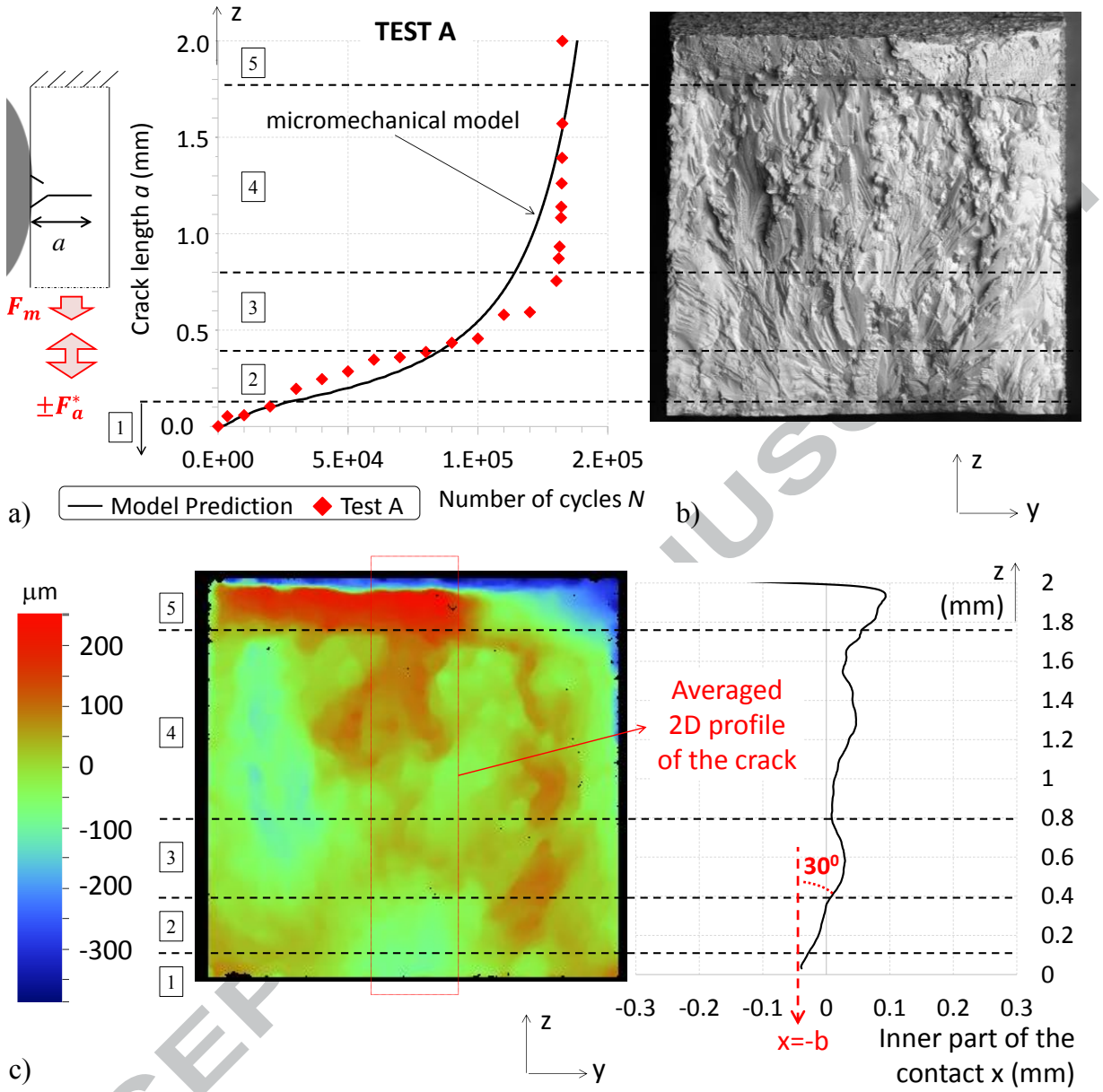


Figure 4: Crack path analysis of Test A (along the z axis) (a) evolution of the projected crack length $\boldsymbol{a}$ at the trailing contact border defined from X-ray radio analysis (b) SEM (back scattered electron mode) image of the fractured surface (trailing contact border) (c) 3D profile in the inner part of the contact. Extraction of an averaged 2D profile of the crack path. ($\boldsymbol{p_{max} = 300MPa, q_{mqx} = 310MPa, \sigma_a = 59.6MPa, R_{fa} = 0.29, N_f = 132521}$) [31]

### *2.4. FEM modelling*

The loading conditions imposed by the micro fretting fatigue setup are complex and cannot be addressed using analytical formulations [32]. The fretting fatigue experiment is therefore described using a 2D plane strain elastic finite element model (Abaqus software) described in Figure 5 simulating the experimental conditions (more details on the model are available in [31]). The model is composed of a moving steel cylinder ($r = 10mm$), the aluminium sample, and a fixed roller bearing on its back. The mesh uses triangular (CPE3) linear elements outside the contact. The mesh size is then refined down to $1\mu m$ at the contact interface with quadrilateral (CPE4R) linear elements (Figure 5.a). The friction at the interface is described using Lagrange multipliers with the friction coefficient $\mu_t = 1.3$ previously experimentally determined.

The applied loads are presented in Figure 5.b. The mean fatigue load $F_m$ is imposed, followed by the normal load $P$. As we are dealing with a mono-actuator where fretting and fatigue are in phase, fretting fatigue loads are then applied at the same time during one and a half cycle by adding alternative amplitudes, namely $\pm F_a^*$ for the fatigue, and $\pm Q^*$ for the fretting. As described in Figure 5.c, due to the complex fretting fatigue loadings, the shear and pressure distributions are very disturbed and require FEM computations.

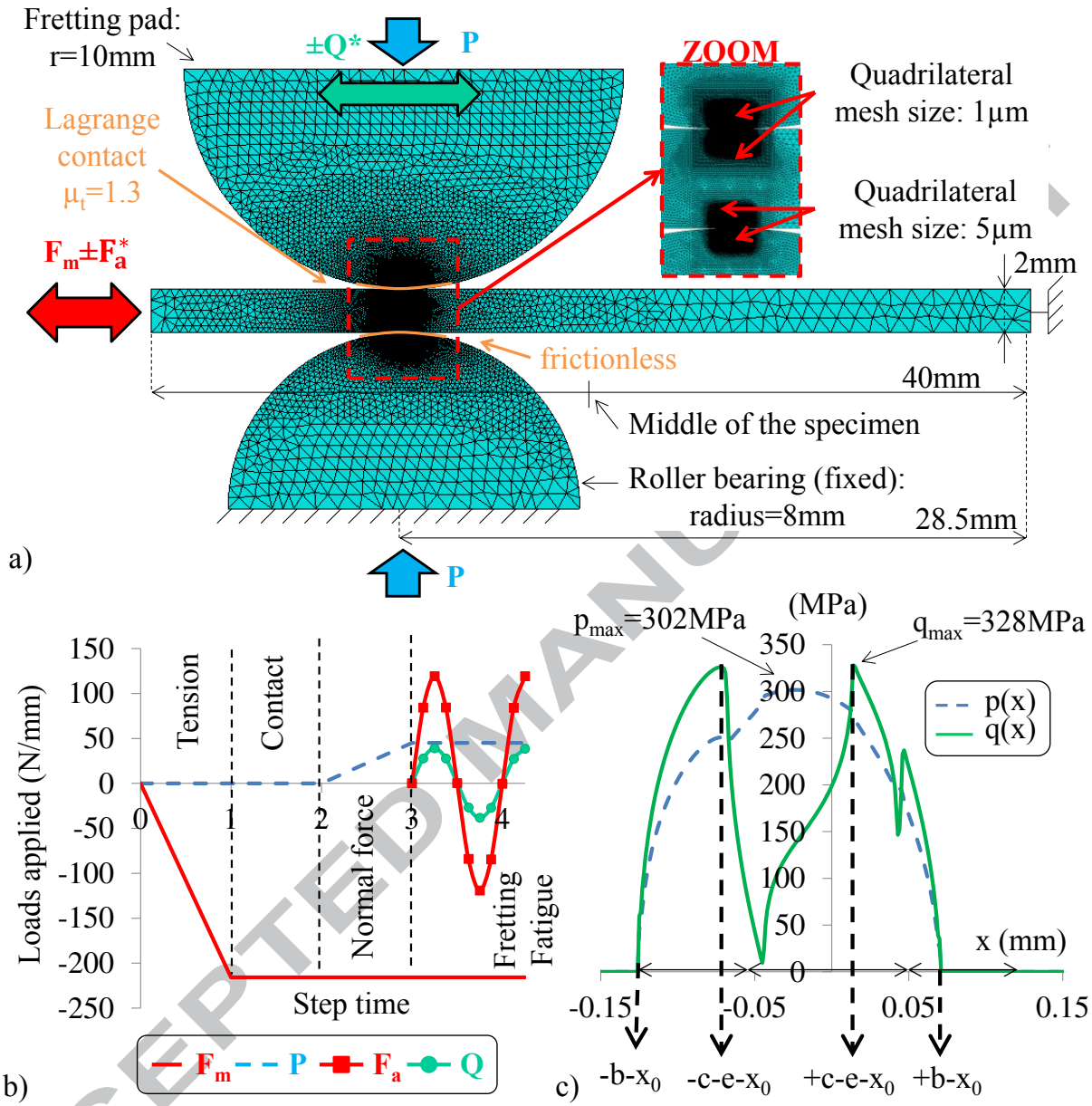


Figure 5: FE modeling of the micro fretting fatigue experiments (a) FE contact description, (b) loading sequence on an elastic configuration (Test A). The stress within the fretting fatigue specimen is maximum when $\boldsymbol{Q(t) = -Q^*}$ as $\boldsymbol{F = F_m - F_a^*}$ and minimum when $\boldsymbol{Q(t) = +Q^*}$ as $\boldsymbol{F = F_m + F_a^*}$. (c) Micro fretting fatigue experiments: surface shear and pressure distributions at the maximum stress level from the FE simulation [31] (with $\boldsymbol{b}$ the half-width contact, $\boldsymbol{c}$ the half-width sticking zone, $\boldsymbol{x_0}$ the eccentricity due to fatigue)

The stress intensity factors of the fretting fatigue crack are computed using a dedicate 2D-plane strain FE model coupled with an automatic remeshing procedure using Matlab and previously described in [31]. A kinked crack shape defined from the synchrotron radiographies is implemented in the previously exposed FEM contact modelling at $x = -b$ where propagation occurs according to Figure 4.a. A friction coefficient between the crack lips $\mu_{crack} = 0.78$ is

used as described in [33]. A single crack is computed at the trailing contact border $x = -b$ at the two stages corresponding to the most severe stress conditions: the stress intensity factor $K_{+Q^*}$ is extracted at $(Q = +Q^*, F = F_m + F_a^*)$ and $K_{-Q^*}$ is extracted at $(Q = -Q^*, F = F_m - F_a^*)$ using the Rice's integrals method (Figure 6, [31, 33]). Note that due to the bending phenomena induced by the fixed roller bearing, the mode I maximum $K_{Imax}$ and minimum $K_{Imin}$ values will occur either at $Q = \pm Q^*$ depending on the crack length so that the stress ratio characterizing at the equivalent fretting fatigue crack tip $R_{eq}$ can be expressed as follows:

$$\begin{cases} R_{eq} = \frac{K_{I,-Q^*(CI)}}{K_{I,+Q^*(CI)}} \; if \; K_{I,-Q^*(CI)} \leq K_{I,+Q^*(CI)} \\ R_{eq} = \frac{K_{I,+Q^*(CI)}}{K_{I,-Q^*(CI)}} \; if \; K_{I,+Q^*(CI)} \leq K_{I,-Q^*(CI)} \end{cases} \quad (2)$$

where $K_{I,-Q^*(CI)}$ and $K_{I,+Q^*(CI)}$ are numerical stress intensity factor values calculated by the Rice's integrals method.

The mode I stress intensity factor range (i.e. $\Delta K_I$) is computed using equation (3). Only the positive part of $K_I$ is considered (a negative value corresponding to a closed crack is not contributing to the propagation).

$$\begin{cases} \Delta K_I = K_{I,+Q^*} \; if \; R_{eq} < 0 \\ \Delta K_I = K_{I,+Q^*} - K_{I,-Q^*} \; if \; R_{eq} > 0 \end{cases} \quad (3)$$

The mode II contribution is expressed by:

$$\Delta K_{II} = K_{II,+Q^*} - K_{II,-Q^*} \; with \; \mu_{crack} = 0.78 \quad (4)$$

An equivalent mixed mode stress intensity factor is therefore considered:

$$\Delta K_{eq} = \sqrt{\Delta K_I^2 + \Delta K_{II}^2} \quad (5)$$

The crack growth rate $da/dN$ between cycles $N_i$ and $N_{i+1}$ where the crack length changes from $a_i$ and $a_{i+1}$ is defined by equation (6) in agreement with the ASTM E647 [31, 34]:

$$\frac{da}{dN} = \frac{a_{i+1} - a_i}{N_{i+1} - N_i} \quad (6) \text{ and } \Delta K_{eq} = \frac{\Delta K_{eq,i+1} - \Delta K_{eq,i}}{2} \quad (7)$$

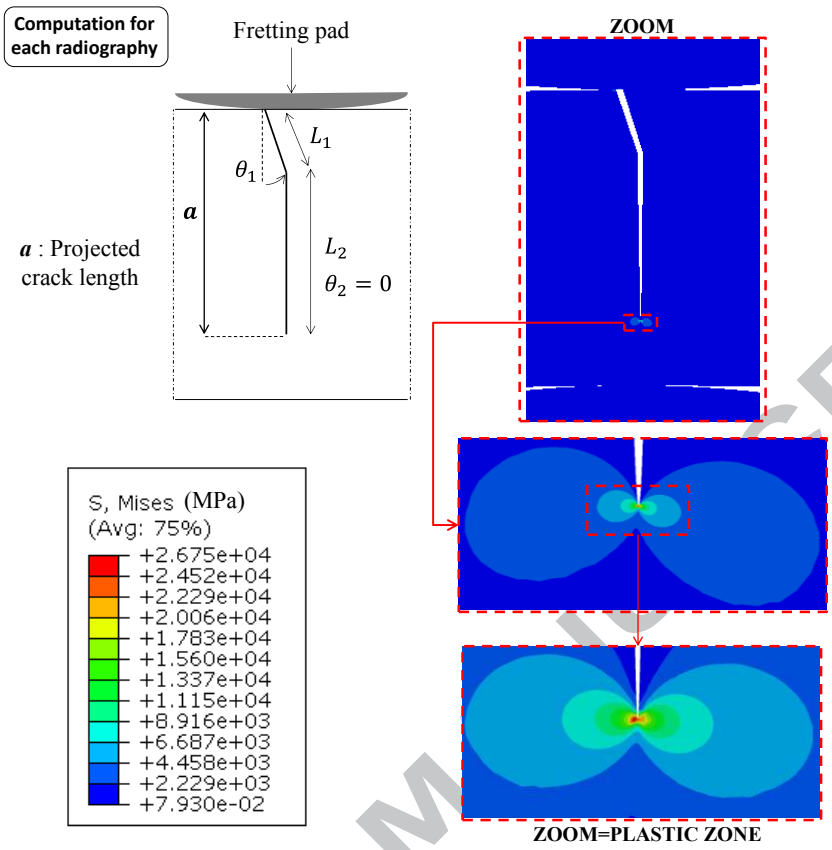


Figure 6: Micro fretting fatigue FEM cracked modelling (Test A after 132521 cycles, at $-\boldsymbol{Q}^*$ and $\boldsymbol{F} = \boldsymbol{F_m} - \boldsymbol{F_a^*}$): schematic configuration and zoom at the crack tip illustrating the monotonic plastic zone for a crack length measured just before failure

### *2.5. Crack growth analysis*

The X-ray radio conditions of Test A are simulated and the corresponding crack growth rate is reported in the $da/dN - \Delta K_{eq}$ diagram (Figure 7). These micro fretting fatigue crack growth rates are compared to the conventional C(T) experiments of the studied 7050-T7451 aluminum alloy.

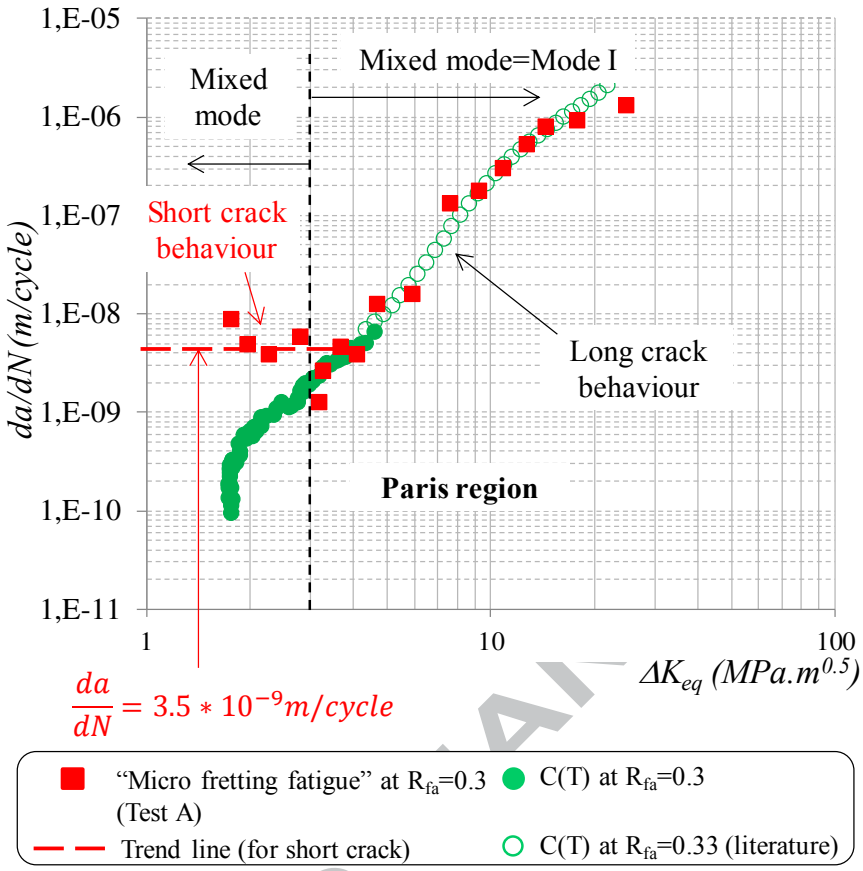


Figure 7: Correlation between micro fretting fatigue experiment and conventional C(T) tests for the 7050-T7451 aluminum alloy (Micro fretting fatigue at $\boldsymbol{R_{fa} = 0.3}$ [31], C(T) at $\boldsymbol{R_{fa} = 0.3}$ [29], C(T) at $\boldsymbol{R_{fa} = 0.33}$ [35])

Focusing on the long crack regime ($\Delta K_{eq} > 3MPa\sqrt{m}$) it is interesting to note that "micro fretting fatigue" crack growth rates are very close to those obtained with macro C(T) experiments following a linear trend on a log-log scale so that a Paris equation can be fitted:

$$\frac{da}{dN} = A_1(\Delta K_{eq})^{m_1} \qquad (8)$$

with $A_1 = 2.94 * 10^{11} m/(cycle.MPa\sqrt{m})$ and $m_1 = 3.78$.

As developed in [31], it confirms the stability of the micro fretting fatigue experiment to characterize long crack behaviours. However, for cracks smaller than $a = 400\mu m$, a short crack behavior is observed. A nearly constant crack growth rate is obtained so that:

$$For\ 0.3 < \Delta K_{eq} < 3MPa\sqrt{m}, \frac{da}{dN} \approx 4.5 * 10^{-9} m/cycle \qquad (9)$$

This transition from low to high $\Delta K_{eq}$ domain is limited in many aspects. First it requires a discontinuous formulation which is not suitable for an optimal numerical model. Secondly it does not explicit the transition from short to long crack propagation regimes which is in fact the controlling factor of such crack growth rate formulation.

### 2.6. Short Crack Correction (SCC) model

Former investigations focusing on the crack arrest conditions conclude that the stress intensity factor range threshold value is not constant and may be expressed as a function of the crack length [36]. Hence, considering the Kitagawa-Takahashi (K-T) diagram, Araújo and Nowell suggested that the stress intensity factor range threshold may be expressed through a discontinuous formulation so that:

$$\begin{cases} \Delta K_{th} = \Delta K_0 \sqrt{\frac{a}{a_0}} \; if \; a < a_0 \\ \Delta K_{th} = \Delta K_0 \; if \; a \geq a_0 \end{cases} \quad (10)$$

With $\Delta K_0$ the long crack threshold and $a_0$ the transition from short to long crack regime previously approximated by equation (1).

Using the El Haddad *et al.* approach, they also derived a more continuous formulation so that whatever the crack length $a$:

$$\Delta K_{th} = \Delta K_0 \sqrt{\frac{a}{a+a_0}} \quad (11)$$

A similar modified short crack growth expression was successively suggested by Pugno *et al.* [37] and by Fleury *et al.* [17] to provide a generalized Paris equation for fatigue crack growth:

$$\Delta K_{eq(SC)} = Y_1 \Delta\sigma \sqrt{\pi(a+a_0)} = Y_1 \Delta\sigma (\pi a (1+\tfrac{a_0}{a}))^{0.5} \quad (12)$$

Where $Y_1$ is the geometrical parameter, and for surface crack $Y_1 = 1.1215$.

This equivalent short crack stress intensity factor range value can be related to the nominal one according that:

$$\Delta K_{eq} = Y_1 \Delta\sigma \sqrt{\pi a} \quad (13)$$

So that:

$$\Delta K_{eq(SC)} = Y_1 \Delta\sigma \sqrt{\pi a} \sqrt{1+\frac{a_0}{a}} = \Delta K_{eq} \sqrt{1+\frac{a_0}{a}} \quad (14)$$

This short crack modified stress intensity factor range can easily be integrated within the Paris equation:

$$\frac{da}{dN} = A_1 (\Delta K_{eq(SC)})^{m_1} = A_1 \Delta K_{eq}^{m_1} (1+\tfrac{a_0}{a})^{\frac{m_1}{2}} \quad (15)$$

A more general formulation can be considered:

$$\frac{da}{dN} = A_1 \Delta K_{eq}^{m_1} (1+\tfrac{a_0}{a})^{m_{SC}} \quad (16)$$

With $m_{SC}$ an exponent conditioning the short crack correlation. When $m_{SC} = 0$, no short crack correction is considered whereas $m_{SC} = m_1/2$ corresponds to the El Haddad description.

Figure 8 compares the proposal versus the studied micro fretting fatigue analysis. Like previously underlined, the plain $\Delta K_{eq}$ (ie. for $m_{SC} = 0$) formulation is unable to capture the short crack response. The El Haddad approach ($m_{SC} = m_1/2 \approx 1.9$) improves the correlation but the constant crack growth rate in the small $\Delta K_{eq}$ domain is not described. The model extrapolates a crack growth rate around the order of magnitude of $10^{-9} m/cycle$ for

$\Delta K_{eq} = 2MPa\sqrt{m}$ against $10^{-8}m/cycle$ for the experiment. Hence the El Haddad approximation of $m_{SC}$ can lead to dangerous underestimation of the short crack growth rate.

A parametric analysis is done and shows that the short crack rate is better approximated when $m_{SC} = 6$ which implies:

$$\frac{da}{dN} = A_1 \Delta K_{eq}^{m_1} (1 + \frac{a_0}{a})^6 \qquad (17)$$

This rather high $m_{SC}$ value is physically questionable but provides a better description of the global short to long crack growth rate response.

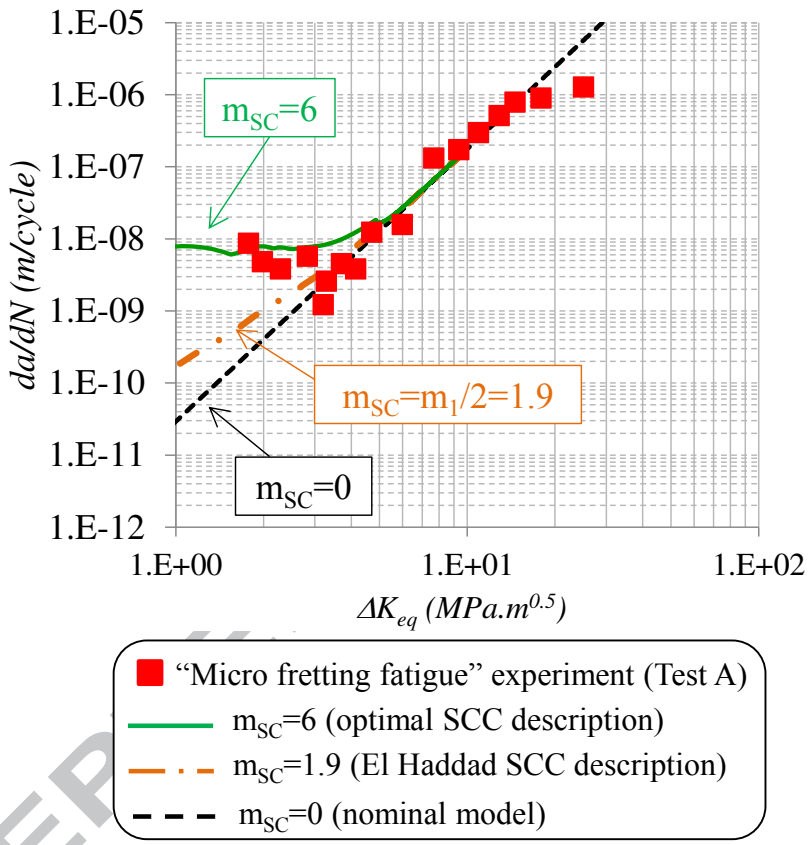


Figure 8: Comparison between the proposed Short Crack Correction (SCC [17, 37]) and the studied micro fretting fatigue analysis (Test A [31])

This short crack correction of the crack growth rate formulation is simply very practical to predict the crack propagation evolution but is limited in many aspects. First the rather high value found for $m_{SC} = 6$ is physically questionable. Secondly the approach does not consider the microstructural effect influencing the discontinuous evolution of the short crack propagation. Hence an alternative microstructural strategy needs to be considered to better illustrate this aspect.

## 3. Microstructural crack propagation model

### *3.1. Navarro-Rios (NR) model: principles*

The proposed model is using the Navarro-Rios formulation detailed in [18-20] which was extended by Vallellano *et al.* [23, 24] later on. The main idea is that a crack and its plastic zones need to overcome microstructural barriers of the material in order to propagate. The present work uses Navarro-Rios hypothesis assuming that only the monotonic plastic zone can be blocked at a grain boundary acting as a barrier, and is responsible for the crack arrest or propagation. By making the sum of stresses applied on the crack, one can calculate the Crack Tip Opening Displacement (CTOD) which is related to the crack growth rate.

Figure 9 illustrates the model principles with the loads involved. A fatigue crack of a $2a$ length initiates within a grain displaying an average size $D$ and propagates in mode I. The crack is subjected to cyclic fatigue loads with a maximal external stress $\sigma_{max}$ tending to open the crack. The latter also deals with $\sigma_1^i$ which is the stress opposed to opening and closing, $\sigma_2^i$ is the stress opposed to deformation and $\sigma_3^i$ is the stress needed to propagate. $\sigma_1^i$ usually represents residual stresses and will not be considered in the present work. The present model uses an odd parameter $i$ representing the half grain interval while the crack propagates ($i = 1, 3, 5 \ldots$). The crack will grow until its monotonic plastic zone reaches a grain boundary at $x = \frac{iD}{2}$ acting like a microstructural barrier where it is blocked. The monotonic plastic zone needs to overcome the first dislocation at $\frac{iD}{2} + r_0$ (with $r_0 \to 0$), where $\sigma_3^i$ is the associated stress, right after the grain boundary so that the crack can propagate.

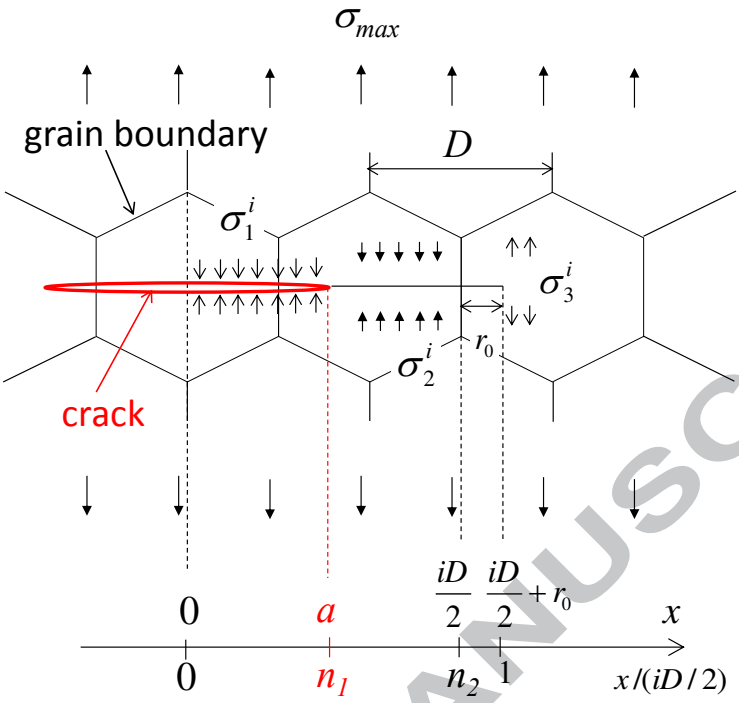


Figure 9: Schematic description of the Navarro-Rios model where $\boldsymbol{D}$ is the average grain size, $\boldsymbol{i}$ the half grain interval, $\boldsymbol{a}$ the crack, $\boldsymbol{\sigma_{max}}$ the maximal external stress, $\boldsymbol{\sigma_1^i}$ the stress opposed to opening and closing, $\boldsymbol{\sigma_2^i}$ the stress opposed to deformation, $\boldsymbol{\sigma_3^i}$ the stress needed to propagate, $\boldsymbol{r_0}$ the distance between grain boundary and the first dislocation [18-20, 38]

The model uses a non-dimensional crack length and is given by (see Figure 9):

$$n_1^i = \frac{a}{iD/2} \qquad (18)$$

The monotonic plastic zone occurring at the crack tip grows within the grain, is blocked by a barrier, and jumps after each grain boundary. Therefore the crack needs to grow within the monoplastic zone blocked at a barrier, before expanding within the following grain. The growth is then determined by the CTOD value described by [20, 24]:

$$\Phi^i = \frac{4}{\pi^2 E'}\sigma_{max}\pi a\left[\frac{\sigma_2^i}{\sigma_{max}} ln\left(\frac{1}{n_1^i}\right) + \frac{\pi}{2}\frac{\sqrt{1-(n_1^i)^2}}{n_1^i}\left(1-\frac{2}{\pi}\left(\frac{\sigma_2^i}{\sigma_{max}}\right)cos^{-1}n_1^i\right)\right] \qquad (19)$$

where, for plane strain conditions:

$$' = \frac{E}{1-\upsilon^2} \qquad (20)$$

According to Curtis *et al.* $\sigma_2^i$ can be approximated by the cyclic yield ($\sigma_2^i \approx \sigma_y$) [38].

The crack growth rate is a function of the CTOD and is given by:

$$\frac{da}{dN} = A_2\Phi^{m_2} \qquad (21)$$

where $A_2$ and $m_2$ are parameters experimentally determined as we will see in the following section.

A threshold condition is reached at a grain boundary and is given by the non-dimensional critical crack length $n_1^i\big|_C$ [23, 24, 39]:

$$n_1^i\big|_C = cos\left(\frac{\pi}{2}\frac{\sigma_{max}-\sigma_{th}^i}{\sigma_2^i}\right) \qquad (22)$$

where $\sigma_{th}^i$ is the maximum stress threshold. The latter should be obtained from the experiment. Nevertheless, as proposed by Vallellano *et al.* [21, 22], it can be approximated by:

$$\sigma_{th}(a) = \sigma_{fl}\frac{{a_0}^{1/2}}{(a^f + {a_0}^f - \left(\frac{D}{2}\right)^f)^{1/(2f)}} \qquad (23)$$

with the crack length $a_0$ is the short-long crack transition obtained in equation (1).

where $\sigma_{fl}$ is the fatigue limit of the material at the corresponding stress ratio, and $f$ is a parameter equal to 2.5 for aluminium alloys as specified by Vallellano *et al.* [21, 22].

Finally, if the monotonic plastic zone is able to overcome the grain boundary, meaning that the crack can propagate within the following grain, then the following step is given by:

$$n_1^{i+2} = n_1^i\big|_C \qquad (24)$$

The number of cycle $N$ is then extracted by integrating Equation (21), namely:

$$N = \frac{1}{A_2}\sum_i \int_{a_s}^{a_c}\frac{da}{\Phi^{m_2}} \qquad (25)$$

where $a_s$ corresponds to the "starting" crack length within grain $i$ and $a_c$ is the "critical" crack length corresponding to the crack reaching the next grain boundary.

### *3.2. Application to fretting fatigue stressing using the FE modelling of the micro fretting fatigue experiments*

Stresses are extracted at the exact contact border $x = -b = -0.099mm$, where maximum stress gradients occur. As a rather straight crack path is experimentally observed we will focus on the mode I propagation, so that only the first component $\sigma_{11}$ of the stress tensor will be considered.

Figure 10.b plots the obtained maximum $\sigma_{max}$ and range $\Delta\sigma = \sigma_{max} - \sigma_{min}$ stresses as functions of the distance $z$ from the surface related to Test F. The corresponded stress ratio $R = \sigma_{min}/\sigma_{max}$ is also added. It is clear that high stress gradients specially appear near the surface ($z \approx 0$), leading to a variable stress ratio. Such variations have to be taken into account into the presented micromechanical fretting fatigue life model as they have a significant influence on the crack propagation.

As reminded by Aguirre *et al.* [40], an equivalent stress has to be considered in order to take into account stress gradients, variable stress ratio and the crack nucleation at an edge. Vallellano *et al.* previously determined such an equivalent stress [39] using the following expression:

$$\sigma_{eq}(a) = Y_2 \frac{2}{\pi} \int_0^a \frac{(1+f(z/a))\sigma(z)}{\sqrt{a^2-z^2}} dz \qquad (26)$$

where $Y_2$ is the correction factor and $f(z/a)$ is a polynomial expression determined from the FEM [41]:

$$f(z/a) = \left(1 - \left(\frac{z}{a}\right)^2\right)\left[0.2945 - 0.3912\left(\frac{z}{a}\right)^2 + 0.7685\left(\frac{z}{a}\right)^4 - 0.9942\left(\frac{z}{a}\right)^6 + 0.5094\left(\frac{z}{a}\right)^8\right] \qquad (27)$$

Figure 10 shows the calculation procedure to obtain equivalent stresses. The FE model exposed in Figure 5 is first computed. At the studied fretting fatigue load stage, $\sigma_{11}$(maximum, minimum, or both) is extracted at the exact contact border where the stress is maximum ($x = -b = -0.099mm$). Equation (26) is applied on the extracted stress to finally be able to plot the equivalent stress $\sigma_{eq}$ as a function of the depth.

The maximum equivalent stress $\sigma_{eq,max}$ and the equivalent stress range $\Delta\sigma_{eq} = \sigma_{eq,max} - \sigma_{eq,min}$ are introduced in the micostructural model by replacing $\sigma_{max}$ with $\sigma_{eq,max}$ and $\Delta\sigma$ with $\Delta\sigma_{eq}$.

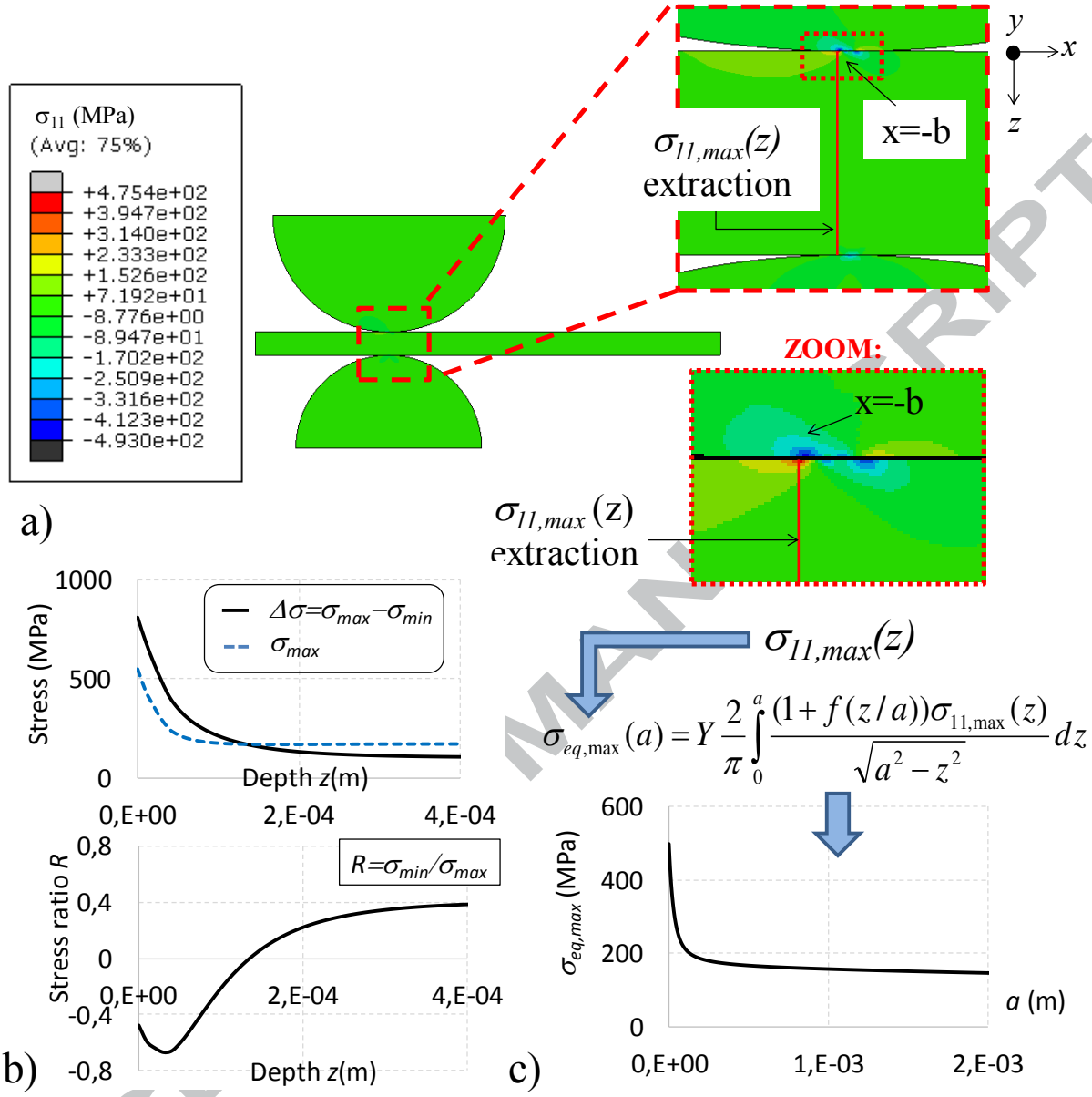


Figure 10: Equivalent stress extraction procedure (a) FE modeling with the stress extraction $\boldsymbol{\sigma_{11}}$ at the contact border $\boldsymbol{x = -b}$ along the depth $\boldsymbol{z}$ (Test A) and at the maximum fretting fatigue load stage, (b) Stress range variation $\boldsymbol{\Delta\sigma}$ and the corresponding stress ratio $\boldsymbol{R_{eq}}$ as a function of the depth $\boldsymbol{z}$ (c) Maximum equivalent stress calculation (Test A) [39, 40] (Test A: $\boldsymbol{p_{max} = 300MPa, q_{mqx} = 310MPa, \sigma_a = 59.6MPa, R_{fa} = 0.29, N_f = 132521}$cycles)

### *3.3. Parameters calibration*

The proposed model uses an initial defect to start the computation of the crack extension. This value is material dependent and has a significant impact on the life prediction. Even if it is known that $5\mu m$ is a representative inclusion size [42], Aguirre *et al.* [40] reminded that it is essential to perform a deeper investigation on this value. Thus a parametric study on the initial

defect was preliminary performed in order to check the model stability. It appeared that for a defect larger than $5\mu m$, there is a drastic drop of the life prediction, whereas for defects between $2\mu m$ and $5\mu m$, small variations are observed. For defects smaller than $2\mu m$, no variation is observed. Assuming that fretting crack nucleation is led by severe stress gradients more than microstructural effects within the very early stage, an initial defect of $1\mu m \ll D$ will be used for the computations.

The $\sigma_2$ variable was related to $\sigma_y$ so that $\sigma_2 = \sigma_y = 80MPa$. The crack shape correction used in Equation (26) was set to $Y_2 = 0.805$ corresponding to the theoretical value for semi-elliptical cracks [40, 43]. The so called "Navarro-Rios coefficients" $A_2$ and $m_2$ in equation (21) are determined with the experiment by fitting the LEFM long crack regime [23, 24]. Therefore the following equivalence can be made for long cracks:

$$\frac{da}{dN} = A_2 \Phi^{m_2} = A_1 \Delta \mathrm{K}^{m_1} \qquad (28)$$

The presented model was first computed using only fatigue loads in order to determine the "Navarro-Rios coefficients" $A_2$ and $m_2$ at the stress ratio $R_{fa} = 0.3$. Figure 11 plots the crack growth rate $da/dN$ as a function of the stress intensity factor range $\Delta K$ with $\Delta K = \Delta\sigma\sqrt{\pi a}$. Figure 11 compares experimental data extracted from fatigue crack growth tests [28, 29] for long cracks performed at $R_{fa} = 0.3$ and the corresponding micromechanical small fatigue crack growth model. The long crack regime is fitting the experiment by taking $A_2 = 260$ (1/cycles) and $m_2 = 1.78$ (-).

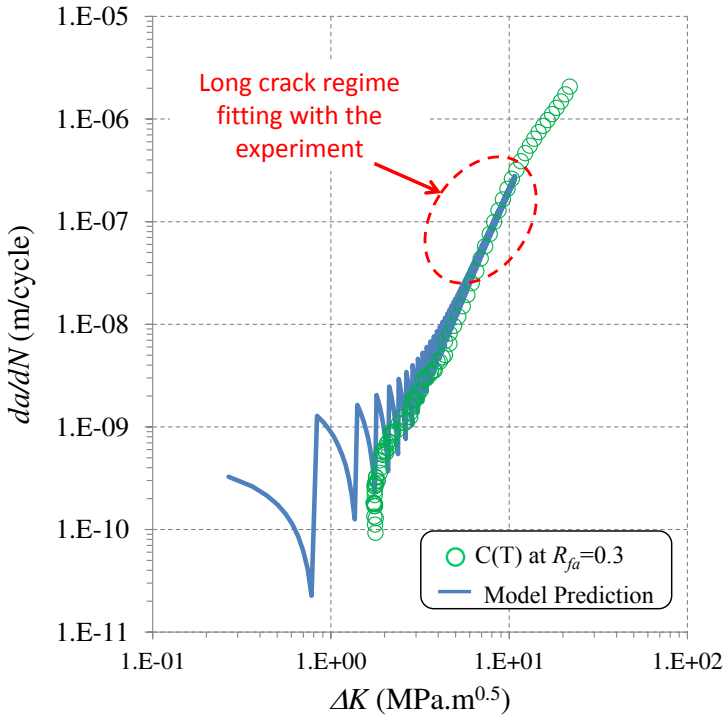


Figure 11: Fatigue crack growth: model prediction versus experimental data at the stress ratio $\boldsymbol{R_{fa} = 0.3}$ [29, 35]

## 4. Comparison between fretting fatigue experiments and micromechanical modelling

### *4.1. $da/dN - a$ representation*

Figure 12.a displays the in situ fretting fatigue data obtained at the synchrotron facility related to Test A. It appears that the experimental points seen on the ESRF radios are very close to the prediction line, which even enables us to identify the five zones observed on the SEM (Figure 4). During the first zone, the crack nucleation is driven by fretting loadings which generate acceleration. Arriving on the second zone, deeper within the sample, the crack decelerates as the crack tip is less influenced by fretting, creating an inflection point between the first and second zones. The third zone is crucial as this is where fatigue becomes the main driving parameter making the crack grow. Thereby the crack will drastically accelerate until failure of the specimen. By comparison, Figure 12.b shows the same trends on Test B. The latter was not in situ performed but the SEM observations are making the five zones identifiable on the crack growth predicted curve.

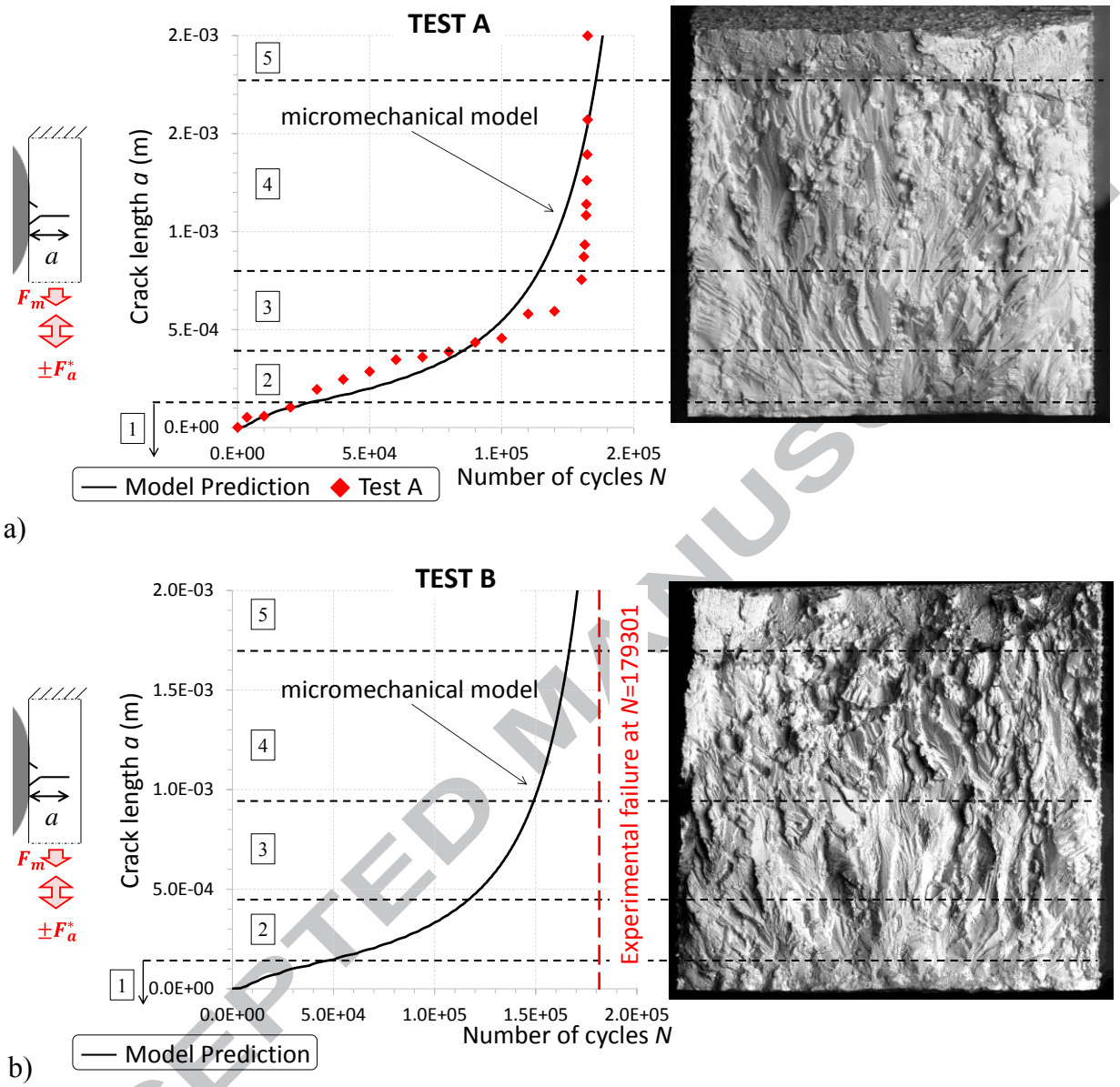


Figure 12: Fretting fatigue crack length evolution $\boldsymbol{a}$ as a function of the fretting fatigue cycles $\boldsymbol{N}$ and comparison versus SEM fracture surfaces (correlation versus fractographic features 1 to 5)) (a) In situ fretting fatigue crack propagation observation (Test A) versus the model prediction, (b) Model prediction versus experimental failure (Test B)

The fretting and fatigue contributions can be analyzed thanks to Figure 13 by plotting the crack growth $da/dN$ for both tests B and A as a function of the crack length $a$. The continuous line represents Test A whereas dashes are related to Test B. For both tests, a first acceleration occurs, validating the observations made on Figure 12. The crack then decelerates around $100 - 150\mu m$ which exactly corresponds to the transition from the first to the second zone. The crack is obviously lead by fretting from its initiation up to $100 - 150\mu m$. In this region, the curve corresponding to Test B is below the one obtained for Test A (Figure 13) which is

coherent with the experiment as Test B displays a lower fretting contribution with a maximum shear stress about $q_{max} = 302MPa$ compared to $q_{max} = 310MPa$ for Test A. When cracks are above $100 - 150\mu m$, fatigue is monitoring the crack growth with a rather straight slope until reaching failure. Again, the curve related to Test B is below the one for Test A as the maximum fatigue stress is lower for Test B with $\sigma_{fat,max} = 162MPa$ versus $\sigma_{fat,max} = 167.5MPa$ for Test A. If those two differences on the fretting and fatigue loadings do not seem to be that significant on a mechanical point of view, they have a dramatic influence on the fretting fatigue life as Test B is longer than Test A with almost 50000 additional fretting fatigue cycles. Thus the short-long crack transition can easily be identified by combining Figure 12 and Figure 13. It appears that the transition is exactly at the one passing from the first to the second zone (Figure 12). The number of cycles related to short and long crack can directly be identified with the proposed model at $N \approx 50000$ cycles for Test B, and $N \approx 20000$ for Test A. Thereby the short and long crack domains represent 30% and 70% respectively for the fatigue life regarding Test B, versus 15% and 85% for Test A.

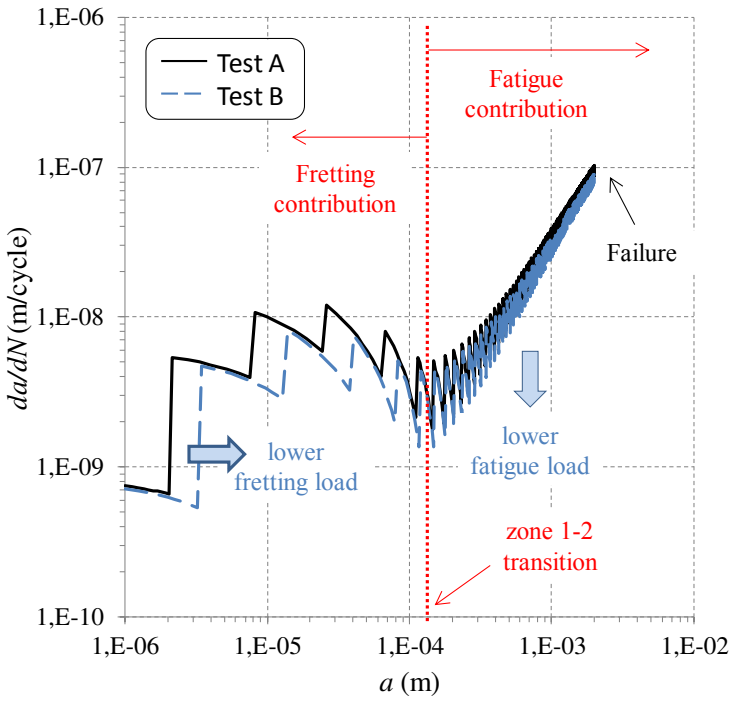


Figure 13: Predicted fretting fatigue crack growth $\boldsymbol{da/dN}$ as a function of the crack length $\boldsymbol{a}$ for Tests B ($\boldsymbol{p_{max} = 300MPa, q_{mqx} = 302MPa, \sigma_a = 54.4MPa, R_{fa} = 0.33, N_f = 179301}$) and Test A ($\boldsymbol{p_{max} = 300MPa, q_{mqx} = 310MPa, \sigma_a = 59.6MPa, R_{fa} = 0.29, N_f = 132521}$)

### *4.2. $da/dN - \Delta K$ representation*

The micromechanical model is based on a $da/dN - a$ crack growth description allowing a more representative analysis of material microstructural effects on short crack propagation. It can also be transposed to the $da/dN - \Delta K$ engineering representation.

Indeed, assuming semi-circular cracks, Akiniwa *et al.* [44] proposed the following equation:

$$\Delta K = 0.77\Delta\sigma\sqrt{\pi a} \qquad (29)$$

In their research work, Akiniwa *et al.* focused on the 2024-T3 aluminum alloy where samples were machined using thin sheets about $3mm$ thick. Therefore the same correction factor can be used in the present work as the studied samples displayed a $2mm$ thickness which is in the same order of specimen thickness. The equivalent stress intensity factor range $\Delta K_{eq}$ can be calculated with:

$$\Delta K_{eq} = 0.77\Delta\sigma_{eq}\sqrt{\pi a} \qquad (30)$$

The corresponding $\Delta K_{eq}$ were computed and compared to the experimental results defined from the FEM-CI stress intensity factor past processing (Figure 14). All curves are converging for the long crack regime. For short cracks, both FE model (red squares) and the micromechanical fretting fatigue life model (black line) are superimposed confirming that the proposed model is relevant for the studied case. By zooming on the short-long crack transition, points related to the FE model based on the LEFM display same trends as the predicted model with a deceleration followed by a drastic acceleration corresponding to the end of the first zone (Figure 12).

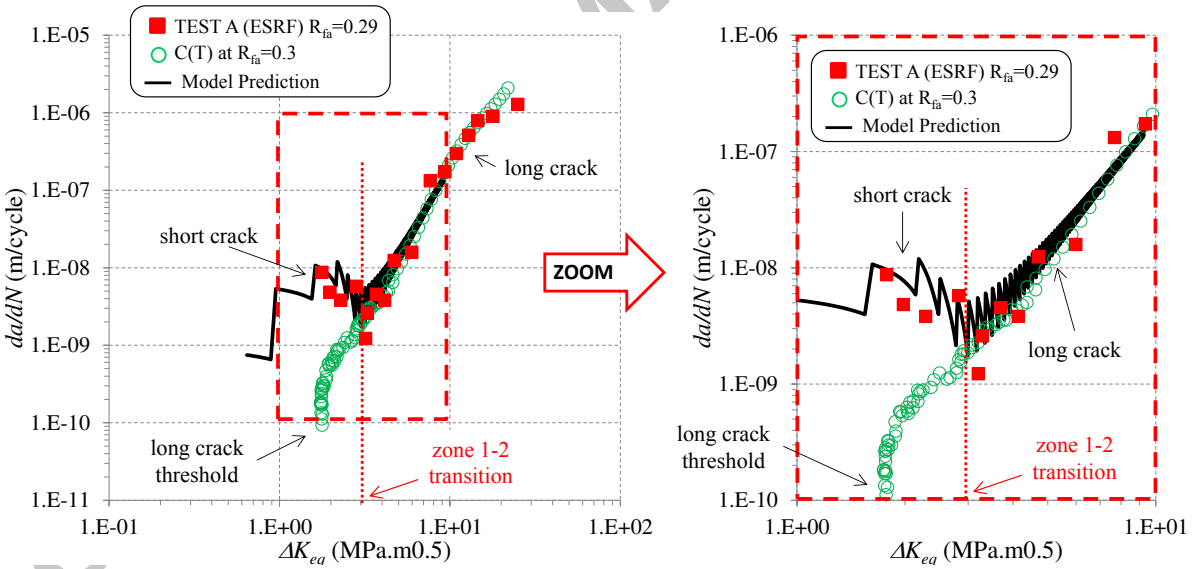


Figure 14: Predicted and experimental small crack propagation curves related to Test A ($\boldsymbol{p_{max} = 300MPa, q_{mqx} = 310MPa, \sigma_a = 59.6MPa, R_{fa} = 0.29, N_f = 132521}$)

### *4.3. Comparison between the Short Crack Correction (SCC) and the Navarro-Rios (NR) approaches*

As previously discussed, the Navarro-Rios approach is the only one able to describe the non-monotonous crack growth evolution when the crack moves from the fretting dominant domain to the deeper fatigue dominant stress domain. To better compare the different modellings, the

evolution of the crack length as a function of the fretting fatigue number of cycles are compared (Figure 15).

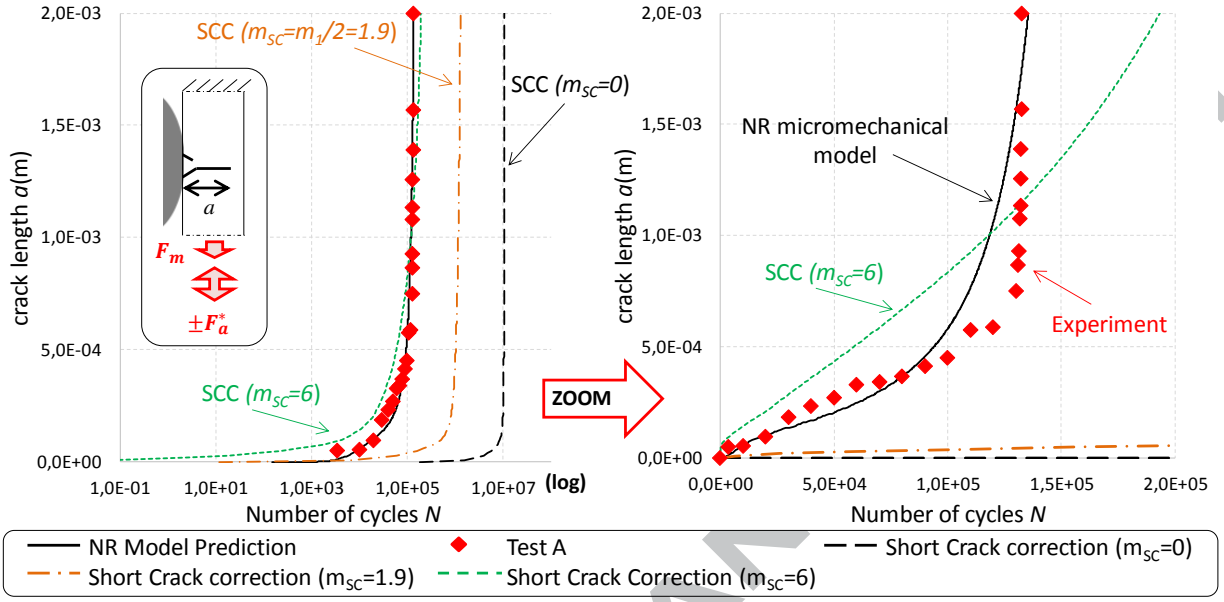


Figure 15: Comparison between experimental (Test A) and simulated evolution of the crack length $\boldsymbol{a}$ as a function of the fretting fatigue cycles $\boldsymbol{N}$ (NR: Navarro-Rios model; SCC: Short Crack Correction with $\boldsymbol{m_{SC}=0}$: no correction, $\boldsymbol{m_{SC}=m_1/2=1.9}$: El Haddad model, $\boldsymbol{m_{SC}=6}$: optimal value obtained from the $\boldsymbol{da/dN-\Delta K_{eq}}$ chart)

The analysis clearly illustrates the very poor correlation given by the plain Paris approximation ($m_{SC}=0$). The El Haddad approach $m_{SC}=m_1/2=1.9$ allows a better prediction and the optimal $m_{SC}=6$ gives a closer estimation of the crack length's evolution, particularly in the very short crack length domain. The best prediction is given by the Navarro-Rios microstructural approach which is able to describe the relative influence of fretting and fatigue stresses.

Another way to analyze the models consists in comparing both predicted and experimental fretting fatigue endurances $N$ and the related relative errors $E(\%)$ (see equation 31, Table 5 and Figure 16):

$$E(\%)=100*\frac{N_{model}-N_{experiment}}{N_{experiment}} \qquad (31)$$

Table 5: Experimental and predicted fretting fatigue lives - Relative errors (%)

| Test | | Experiment (reference) | Short Crack Correction (SCC) | | | Navarro-Rios (NR) |
|---|---|---|---|---|---|---|
| | | | $m_{SC}=0$ | $m_{SC}=1.9$ | $m_{SC}=6$ | |
| A | Number of cycles $N_f$ | 1.33E+05 | 1.08E+07 | 1.27E+06 | 1.93E+05 | 1.38E+05 |
| | Relative error E(%) | - | 8025.73 | 857.04 | 45.83 | 4.32 |
| B | Number of cycles $N_f$ | 1.79E+05 | 1.21E+07 | 1.24E+06 | 2.58E+05 | 1.71E+05 |
| | Relative error E(%) | - | 6664.37 | 592.90 | 43.83 | -4.88 |

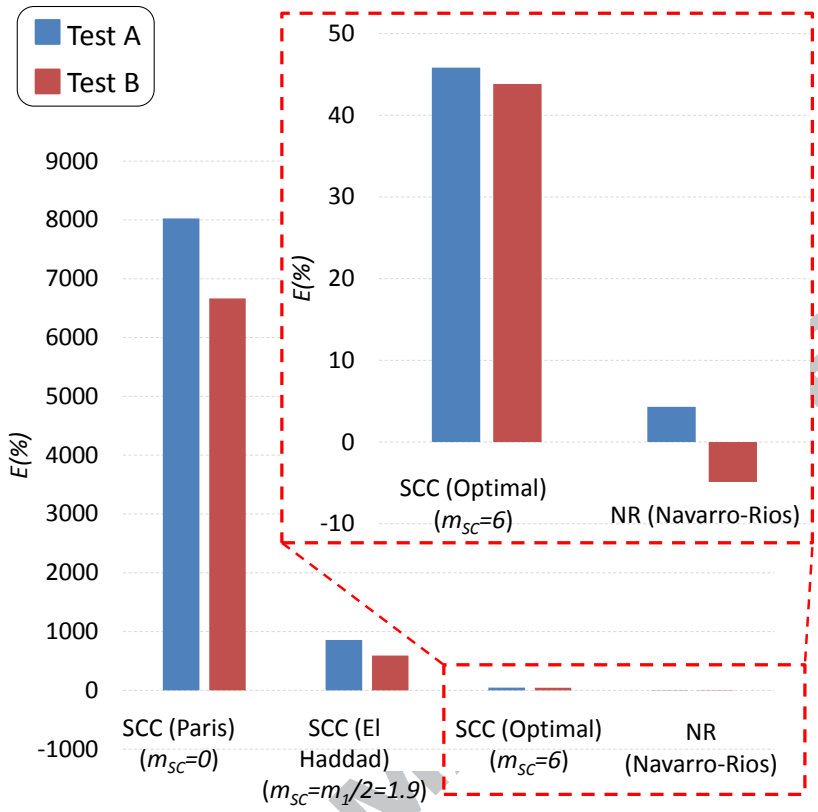


Figure 16: Comparison of the relative errors related to each prediction model

This analysis clearly underlines the stability of the proposed transposition of the Navarro-Rios (NR) model to predict the fretting fatigue crack propagation endurance. It also suggests that despite its simplicity and rather poor physical support of its formulation, the optimal Short Crack Correction (SCC, $m_{SC} = 6$) model allows conservative predictions.

## 5. Conclusions

Using in situ the X-ray synchrotron facility, the fretting fatigue crack growth rate of a 7050-T7451 aluminum alloy was quantified for two specific fretting fatigue loadings. The following points can be highlighted:

- The calculated crack growth rates are consistent with the Paris formulation obtained from conventional C(T) fatigue experiments but differs in the short crack regime (for low $\Delta K_{eq}$) where a rather constant crack growth rate occurs ($da/dN = 4.5 * 10^{-9} m/cycle$ when $\Delta K_{eq} < 3MPa\sqrt{m}$).
- The experimental fretting fatigue analysis shows a discontinuous evolution of the crack propagation in the short crack domain and an unexpected non-monotonous evolution characterized by a deceleration and acceleration when the crack extends deeper below the contact stress influence.

- To capture such peculiar behavior, the Pugno *et al.* and Fleury *et al.* short crack correction strategy, inspired by the El Haddad approach, is applied and rewritten using a basic power expression: $da/dN = A_1 \Delta K_{eq}^{m_1} (1 + a/a_0)^{m_{SC}}$ where $a_0$ is the short-long crack transition.
- The comparison with X-ray micro fretting fatigue results shows that the plain Paris expression ($m_{SC} = 0$) gives dangerous overestimated predictions. The correlation is improved using the original El Haddad approximation ($m_{SC} = m_1/2 = 1.9$). The best prediction is however achieved with $m_{SC} = 6$. This basic approach provides more realistic and conservative predictions, but still requires deeper investigations to explain the high value of $m_{SC}$ the exponent.
- To provide a more physical description of the complex short crack propagation behavior enduring severe stress gradients imposed by fretting stressing, the Navarro-Rios model is transposed: $da/dN - a$ and $da/dN - \Delta K_{eq}$ curves are obtained and show short and long crack behaviours. The curves are well fitting the long crack regime obtained with conventional C(T) fatigue crack growth tests. Additionally the short crack region is perfectly superimposed with data previously obtained thanks to in situ fretting fatigue test analysis.
- The short crack contribution for the total life is smaller than for usual fatigue experiments (from 15% to 30%) and significantly reduces the endurance due to fretting stress gradient effects.
- Despite the fact that the given Navarro-Rios model only considers a mode I description, very good predictions were obtained leading to relative errors inferior to $\pm 5\%$ compared to the experiment.

**Acknowledgments**

The authors thank the Ecole Polytechnique de Montréal, département Génie Mécanique, for the new established partnership with the LTDS and MATEIS, and the Carnot Institute (I@L, project Tomo-Fretting) for financial support.

**References**

[1] E. Eden and W. Rose, "The endurance of metals," in *Proceedings of the Institution of Mechanical Engineers*, 1911, pp. 839-974.

[2] R. Ferre, S. Fouvry, B. Berthel, R. Amargier, and J. A. Ruiz-Sabariego, "Prediction of the Fretting Fatigue Crack Nucleation Endurance of a Ti-6V-4Al/Ti- 6V-4Al Interface: Influence of Plasticity and Tensile/Shear Fatigue Properties," *Procedia Engineering,* vol. 66, pp. 803-812, 2013.

[3] R. Ferré, S. Fouvry, B. Berthel, and J. A. Ruiz-Sabariego, "Stress gradient effect on the crack nucleation process of a Ti–6Al–4V titanium alloy under fretting loading: Comparison between non-local fatigue approaches," *International Journal of Fatigue,* vol. 54, pp. 56-67, 2013.

[4] T. Lindley, "Fretting fatigue in engineering alloys," *International Journal of Fatigue,* vol. 19, pp. 39-49, 1997.

[5] J. A. Araújo, L. Susmel, D. Taylor, J. C. T. Ferro, and J. L. A. Ferreira, "On the prediction of high-cycle fretting fatigue strength: Theory of critical distances vs. hot-spot approach," *Engineering Fracture Mechanics,* vol. 75, pp. 1763-1778, 2008.

[6] J. Araújo and D. Nowell, "Analysis of pad size effects in fretting fatigue using short crack arrest methodologies," *International Journal of Fatigue,* vol. 21, pp. 947-956, 1999.

[7] Z. Zhou, "Fissuration Induite en Petits Débattements: Application au Cas d'Alliages d'Aluminium Aéronautiques," PhD, 1992.

[8] R. Amargier, S. Fouvry, L. Chambon, C. Schwob, and C. Poupon, "Stress gradient effect on crack initiation in fretting using a multiaxial fatigue framework," *International Journal of Fatigue,* vol. 32, pp. 1904-1912, 2010.

[9] J. A. Araújo, G. M. J. Almeida, J. L. A. Ferreira, C. R. M. da Silva, and F. C. Castro, "Early cracking orientation under high stress gradients: The fretting case," *International Journal of Fatigue,* vol. 100, pp. 611-618, 2017.

[10] S. Fouvry, H. Gallien, and B. Berthel, "From uni- to multi-axial fretting-fatigue crack nucleation: Development of a stress-gradient-dependent critical distance approach," *International Journal of Fatigue,* vol. 62, pp. 194-209, 2014.

[11] M. A. Antunes, C. R. M. da Silva, E. M. F. do Rêgo, and A. C. de Oliveira Miranda, "Stress intensity factor solutions for fretting fatigue using stress gradient factor," *Engineering Fracture Mechanics,* vol. 186, pp. 331-346, 2017.

[12] C. Gandiolle, S. Fouvry, and E. Charkaluk, "Lifetime prediction methodology for variable fretting fatigue loading: Plasticity effect," *International Journal of Fatigue,* vol. 92, pp. 531-547, 2016.

[13] R. Hojjati-Talemi, M. Abdel Wahab, J. De Pauw, and P. De Baets, "Prediction of fretting fatigue crack initiation and propagation lifetime for cylindrical contact configuration," *Tribology International,* vol. 76, pp. 73-91, 2014.

[14] E. M. Fontes do Rêgo, M. A. Antunes, and A. C. de Oliveira Miranda, "A methodology for fretting fatigue life estimation using strain-based fracture mechanics," *Engineering Fracture Mechanics,* vol. 194, pp. 24-41, 2018.

[15] M. C. Baietto, E. Pierres, A. Gravouil, B. Berthel, S. Fouvry, and B. Trolle, "Fretting fatigue crack growth simulation based on a combined experimental and XFEM strategy," *International Journal of Fatigue,* vol. 47, pp. 31-43, 2013.

[16] F. Hourlier and A. Pineau, "Propagation of fatigue cracks under polymodal loading," *Fatigue & Fracture of Engineering Materials & Structures,* vol. 5, pp. 287-302, 1982.

[17] R. M. N. Fleury and D. Nowell, "Evaluating the influence of residual stresses and surface damage on fatigue life of nickel superalloys," *International Journal of Fatigue,* vol. 105, pp. 27-33, 2017.

[18] A. Navarro and E. R. de los Rios, "Short and long fatigue crack growth: A unified model," *Phil. Mag.,* vol. 57, pp. 15-36, 1988.

[19] A. Navarro and E. R. de los Rios, "An alternative model for the blocking of dislocations at grain boudaries," *Phil. Mag.,* vol. 57, pp. 37-42, 1988.

[20] A. Navarro and E. R. de los Rios, "Fatigue crack growth modelling by successive blocking of dislocations," *Proc. R. Soc. Lond.,* vol. A437, pp. 375-390, 1992.

[21] C. Vallellano, A. Navarro, and J. domínguez, "Fatigue crack growth threshold coniditons at notches. Part I: Theory " *Fatigue & Fracture of Engineering Materials & Structures,* vol. 23, pp. 113-121, 2000.

[22] C. Vallellano, A. Navarro, and J. Domínguez, "Fatigue crack growth threshold coniditons at notches. Part II: Generalization and application to experimental results," *Fatigue & Fracture of Engineering Materials & Structures,* vol. 23, pp. 128-128, 2000.

[23] C. Vallellano, A. Navarro, and J. Domínguez, "Two-parameter fatigue crack growth driving force: Successive blocking of the monotonic and cyclic plastic zones at microstructural barriers," *International Journal of Fatigue,* vol. 46, pp. 27-34, 2013.

[24] C. Vallellano, J. VÁZquez, A. Navarro, and J. DomÍNguez, "A micromechanical model for small fatigue crack growth: an approach based on two threshold conditions," *Fatigue & Fracture of Engineering Materials & Structures,* vol. 32, pp. 515-524, 2009.

[25] M. Shahzad, M. Chaussumier, R. Chieragatti, C. Mabru, and F. Rezai-Aria, "Surface characterization and influence of anodizing process on fatigue life of Al 7050 alloy," *Materials & Design,* vol. 32, pp. 3328-3335, 2011.

[26] J. Newman, J. Shaw, B. Annigeri, and B. Ziegler, "Fatigue and crack growth in 7050-T7451 aluminium alloy under constant- and variable-amplitude loading," *J. Eng Gas Turb Power,* vol. 135, 2013.

[27] A. R. Moustafa, B. Berthel, S. Fouvry, and E. Charkaluk, "Experimental study of the stress gradient effect under fretting loading by full field measurement techniques," *Wear,* vol. 330-331, pp. 160-169, 2015.

[28] *Military Handbook. Metallic materials and elements for aerospace and vehicle sutructures.*, 1998.

[29] A. de Pannemaecker, S. Fouvry, M. Brochu, and J. Y. Buffiere, "Identification of the fatigue stress intensity factor threshold for different load ratios R: From fretting fatigue to C(T) fatigue experiments," *International Journal of Fatigue,* vol. 82, pp. 211-225, 2016.

[30] J. Meriaux, S. Fouvry, K. J. Kubiak, and S. Deyber, "Characterization of crack nucleation in TA6V under fretting–fatigue loading using the potential drop technique," *International Journal of Fatigue,* vol. 32, pp. 1658-1668, 2010.

[31] A. de Pannemaecker, J. Y. Buffiere, S. Fouvry, and O. Graton, "In situ fretting fatigue crack propagation analysis using synchrotron X-ray radiography," *International Journal of Fatigue,* vol. 97, pp. 56-69, 2017.

[32] D. A. Hills and D. Nowell, *Mechanics of fretting fatigue*, Springer Science & Business Media ed., 1994.

[33] A. de Pannemaecker, S. Fouvry, and J.-Y. Buffiere, "Introduction of a reverse simulation approach to identify the fatigue stress intensity factor crack arrest threshold from fretting cracking experiments," *Tribology International,* vol. 76, pp. 122-132, 2014.

[34] ASTM, "Standard test method for measurement of fatigue crack growth rates," in *vol. E647-13*, ed.

[35] A. Handbook, *Properties and selection: nonferrous alloys and special purpose materials* vol. 2, 1990.

[36] J. Araújo and D. Nowell, "The effect of rapidly varying contact stress fields on fretting fatigue," *International Journal of Fatigue,* vol. 24, pp. 763-775, 2002.

[37] N. Pugno, M. Ciavarella, P. Cornetti, and A. Carpinteri, "A generalized Paris' law for fatigue crack growth," *Journal of the Mechanics and Physics of Solids,* vol. 54, pp. 1333-1349, 2006.

[38] S. Curtis, E. Delosrios, C. Rodopoulos, and A. Levers, "Analysis of the effects of controlled shot peening on fatigue damage of high strength aluminium alloys," *International Journal of Fatigue,* vol. 25, pp. 59-66, 2003.

[39] C. Vallellano, J. domínguez, and A. Navarro, "On the estimation of fatigue failure under fretting conditions using notch methodologies," *Fatigue fract. Eng. Mater. Struct.,* vol. 26, pp. 469-78, 2003.

[40] F. Aguirre, C. Vallellano, and J. Domínguez, "On the application of a micromechanical small fatigue crack growth model to predict fretting fatigue life in AA7075-T6 under spherical contact," *Tribology International,* vol. 76, pp. 6-13, 2014.

[41] R. J. Hartranft and G. C. Sih, "Alternating method applied to edge and surface crack problems," *SihGC, editor. Methods of analysis and solutions of crack problems. Leyden: Noordhoff International Publishing,* pp. 179-238, 1973.

[42] J. Lankford, "The growth of small fatigue cracks in 7075-T6 aluminium," *Fatigue & Fracture of Engineering Materials & Structures,* vol. 5, pp. 233-248, 1982.

[43] G. R. Irwin, "Crack-extension force for a part-through crack in plate," *J. Appl Mech,* vol. 29, pp. 651-654, 1962.

[44] Y. Akiniwa, K. Tanaka, and E. Matsui, "Statistical characteristics of propagation of small fatigue cracks in smooth specimens of aluminium alloy 2024-T3," *Materials Science and Engineering: A,* vol. 104, pp. 105-115, 1988.

- In situ X-ray imaging of micro-fretting fatigue experiments are simulated.
- A Pugno et al./Fleury et al. short crack correction (SCC) approach is considered.
- A microstructural Navarro-Rios (NR) model is transposed.
- Strategies are compared and very good agreement with experiments are observed.
- The NR model provides a more physical description of the short crack behaviour.